Feeble Single Atom Pd Catalyst for H_2 Production from Formic Acid

Esmail Doustkhah,*[,a,b,c] Nao Tsunoji,[d] Shinya Mine,[e] Takashi Toyao,[f] Ken-ichi Shimizu,[f] Tetsuro Morooka,[h] Takuya Masuda,[g,h] M. Hussein N. Assadi,[i] Yusuke Ide*[,a,j]

[a] *Research Center for Materials Nanoarchitechtonics (MANA), National Institute for Materials Science (NIMS), 1-1 Namiki, Tsukuba, Ibaraki 305-0044, Japan, Email: IDE.Yusuke@nims.go.jp*

[b] *Koç University Tüpraş Energy Center (KUTEM), Department of Chemistry, Koç University, Istanbul 34450, Turkey*

[c] *Chemistry Department, Faculty of Engineering and Natural Sciences, Istinye University, 34396 Sarıyer, Istanbul, Turkey, Esmail: esmail.heragh@istinye.edu.tr*

[d] *Department of Applied Chemistry, Graduate School of Advanced Science and Engineering, Hiroshima University, 1-4-1 Kagamiyama, Higashi-Hiroshima 739-8527, Japan*

[e] *National Institute of Advanced Industrial Science and Technology (AIST), Research Institute for Chemical Process Technology, 4-2-1 Nigatake, Miyagino, Sendai 983-8551, Japan*

[f] *Institute for Catalysis, Hokkaido University; Sapporo 001-0021, Japan*

[g] *Graduate School of Chemical Sciences and Engineering, Hokkaido University, Sapporo, Hokkaido 060-0810, Japan*

[h] *Research Center for Energy and Environmental Materials (GREEN), National Institute for Materials Science (NIMS), Tsukuba, Ibaraki 305-0044, Japan*

[i] *RIKEN Center for Emergent Matter Science (CEMS), 2-1 Hirosawa, Wako, Saitama 351–0198, Japan*

[j] *Graduate School of Engineering Science, Yokohama National University, 79-5 Tokiwadai, Hodogaya-ku, Yokohama 240-8501, Japan.*

Keywords: Single atom catalysis (SAC); Pd nanocluster; Silica-supported Pd; Pd DOS; Metal-support interaction; Catalyst reconstruction; Ligand-metal charge transfer; Density functional theory (DFT).

Abstract

Single-atom catalysts are thought to be the pinnacle of catalysis. However, for many reactions, their suitability is yet to be unequivocally proven. Here, we demonstrate why single Pd atoms (Pd_{SA}) are not catalytically ideal for generating H_2 from formic acid as a H_2 carrier. We loaded Pd_{SA} on three silica substrates, mesoporous silicas functionalized with thiol, amine, and dithiocarbamate functional groups. The Pd catalytic activity on amino-functionalized silica (SiO_2-NH_2/Pd_{SA}) was far higher than the thiol-based catalysts (SiO_2-S-Pd_{SA} and SiO_2-$NHCS_2$-Pd_{SA}), while the single-atom stability of SiO_2-NH_2/Pd_{SA} against aggregation after the first catalytic cycle was the weakest. In this case, Pd aggregation boosted the reaction yield. Our experiments and calculations demonstrate that Pd_{SA} in SiO_2-NH_2/Pd_{SA} loosely binds with amine groups. This leads to a limited charge transfer from Pd to the amine groups and causes high aggregability and catalytic activity. According to the density functional calculations, the loose binding between Pd and N causes most of Pd's 4*d* electrons in aminofunctionalized SiO_2 to remain close to the Fermi level and labile for catalysis. However, Pd_{SA} chemically binds to the thiol group, resulting in strong hybridization between Pd and S, pulling Pd's 4*d* states deeper into the conduction band and away from the Fermi level. Consequently, fewer 4*d* electrons were available for catalysis.

Introduction

Pd, known as a powerful noble catalyst, has taken a promising place in various types of catalysis, including oxidation, coupling,[1] cycloaddition,[2] carbonylation,[3] hydrodeoxygenation,[4] and especially in hydrogen generation. While many attempts at investigating the catalysis mechanism through Pd species have been established, some controversies on mechanistic elucidations remain to be answered. The debate over the mechanisms governing Pd catalytic activity mainly originates from the complex interdependent parameters in determining the effective yield, *i.e.*, support's surface chemistry[5] and morphology,[6] the crystallinity and the particle size of Pd, and the reaction conditions. For instance, some argue that the catalytic activity of Pd depends on the basicity of the functional groups on the support surface,[7] while others have reported that the Pd nanoparticles with the ultrasmall size are the best approach that should be sought for obtaining optimal catalysis.[8,9]

In our recent investigation, we demonstrated that the thickness of Pd plate-like nanoparticles on any given support should be investigated to find optimal catalytic performance since the optimal Pd thickness to deliver maximum catalytic activity depends on the type of the support and its surface chemistry.[10] However, how a functional group can influence Pd's electronic structure in conjunction with the support material has rarely been investigated. Additionally, the interdependence of stability and catalytic activity is a further point that requires careful investigation in the case of Pd-supported catalysts possessing a functionalized surface.

A vast fraction of investigations so far have also been focused on reactant/Pd interactions, that is, how potent incoming molecules *vs.* how weak output molecules are.[11–13] However, the interplay between the support and Pd is undeservedly less investigated.[14–17] This latter interaction becomes more significant in determining Pd's electronic structure as the size shrinks as the hybridization with the support strengthens.[10,16]

Single-atom catalysis (SAC) is a recently developed concept that is being widely investigated for several catalytically active metals on various supports for various reactions.[18–22] It has been demonstrated that the support material plays a fundamental role in the catalytic activity of SAC.[23,24] Unlike many other metals synthesized as sing-atom catalysts, which can readily be synthesized, stabilized, and reveal a high efficiency,[25,26] Pd single-atom (Pd_{SA}), requires overly cumbersome synthesis methods and suffers lower stabilization.[19] Furthermore, the ligand-metal charge transfer,[23,24] and the metal-metal interactions[21] are well-established phenomena that must be investigated separately for each species in catalysis, which are also crucial to understanding the catalytic behavior of Pd. As a result, a universal picture regarding the Pd_{SA} catalytic activity and mechanism has not been established so far despite a vast range of investigations.[19,20,27–29]

Herein, we investigate the relationship between the catalytic activity and the stability of Pd_{SA} when supported on different organofunctionalized-mesoporous silicas, *i.e.*, -NH_2, -SH, and -$NHCS_2H$. Pd_{SA} on NH_2 functionality in formic acid dehydrogenation indicates far higher activity than that of Pd_{SA} on thiol-based functionalities, especially at lower temperatures. Density functional calculations demonstrate that the Pd_{SA} binds rather weakly to the -NH_2 group, resulting in an *in situ* aggregation of Pd_{SA} and subsequent enhancement in the metallic feature and charge transfer, and eventually, the catalytic activity improvement (Scheme 1).

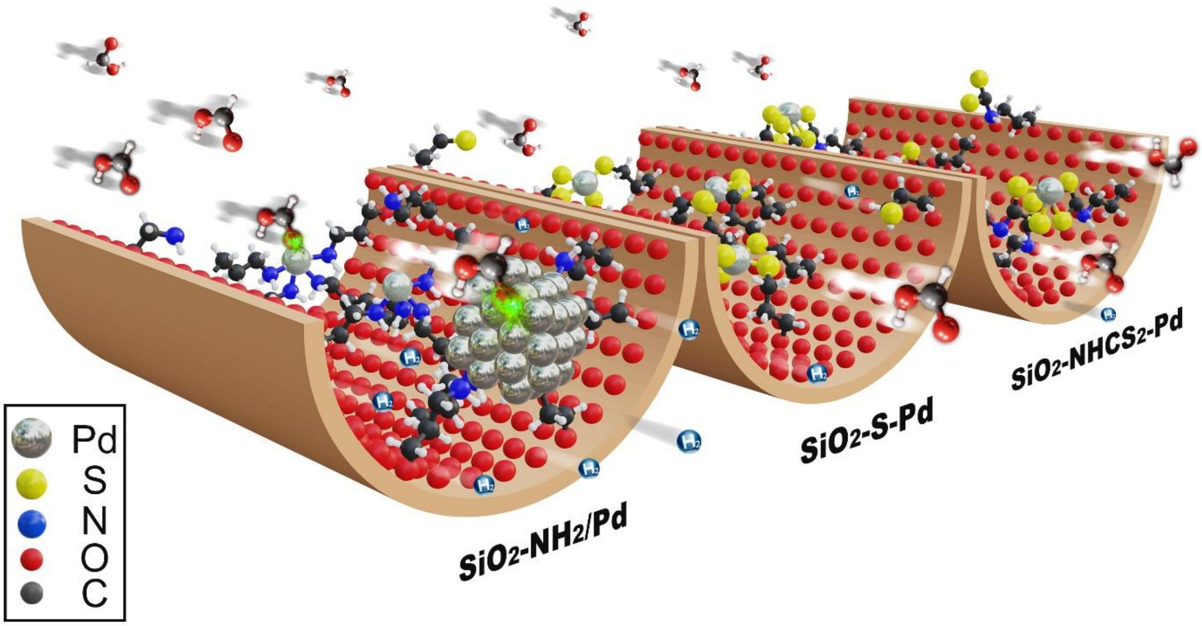

Scheme 1. Schematic view of Pd single atom loaded samples and their catalytic behavior in formic acid dehydrogenation: SiO_2-NH_2/Pd, SiO_2-S-Pd, SiO_2-$NHCS_2$-Pd.

Results and discussions

We first functionalized mesoporous SiO_2, SBA-15, with a pore diameter of 8 nm, with amine (SiO_2-NH_2) and thiol (SiO_2-SH) functional groups to serve as anchoring points for Pd_{SA} and Pd_{NP}. ^{29}Si magic angle spinning nuclear magnetic resonance spectroscopy (MAS NMR) and ^{13}C cross-polarization MAS NMR (CP MAS NMR) (Figure S1A, B) confirmed the successful functionalization of aminopropyl and mercaptopropyl groups on SiO_2 surface via Si-O-Si covalent bands for SiO_2-NH_2 and SiO_2-SH, respectively. The successful functionalization, while retaining the original hexagonally ordered mesoporous structure,[30] was confirmed by low-angle X-ray diffraction (XRD) and N_2 adsorption/desorption (Figure S1C, D). Measuring the thermogravimetric (TG) and differential thermal analysis (DTA) showed that the ratio of functional groups on support SiO_2 are 3.8 and 3.0 mmol per each g of SiO_2, for SiO_2-NH_2 and SiO_2-SH, respectively (Figure S2).

We then deposited Pd species on the functionalized mesoporous silicas. According to the ^{29}Si MAS NMR, the Pd_{SA}-deposited samples (the products are named SiO_2-NH_2/Pd_{SA} and SiO_2-S-Pd_{SA}) show that the ratios of organofunctionalized silanols (T peak, mainly at −66.5 ppm) to free unfunctionalized silanols (Q^3 peak at −100 ppm) hardly changed compared to samples before Pd_{SA} loading (Figure S3A). ^{13}C CP MAS NMR reveals the presence of propylene chains, which link the silica surface to the functional groups constantly before and after the deposition of Pd, as shown in Figure S3B (vs Figure S1B). The low angle XRD patterns and N_2 adsorption-desorption isotherms analyses (surface areas, pore diameters, and pore volumes) (Figures S1C, D & S4, Table S1) also show how the functionalization and subsequent Pd loading on SiO_2 support has affected the SiO_2's porosity and surface area. Accordingly, the surface area, pore volume, and pore size of SiO_2-NH_2 and SiO_2-SH only slightly decreased after Pd deposition. This implies the anchored Pd species are very small in size or amount. According to the elemental analysis, the amounts of loaded Pd in each SiO_2-NH_2/Pd_{SA} and SiO_2-S-Pd_{SA} are found to be 1.4 and 1.1 wt%, respectively (Table S2). Given the amount of grafted functional groups obtained from TG-DTA curves, the Pd to organic functional unit ratios are identical for both SiO_2-NH_2/Pd_{SA} and SiO_2-S-Pd_{SA} and are 1.0:23.0.

As expected, the transmission electron microscopy (TEM) images of SiO_2-NH_2/Pd_{SA} and SiO_2-S-Pd_{SA} detected no Pd nanoparticles, confirming that the deposited Pd species were not aggregated as particles that could be observable under even a high-angle annular dark-field scanning transmission electron microscopy (HAADF-STEM) (Figure 1A–D). Additionally, TEM-based elemental mapping images showed a spatially uniform Pd distribution on the substrate, similar to the nitrogen and sulfur distribution, reaffirming that it was unlikely that the Pd species had aggregated on SiO_2-NH_2/Pd_{SA} and SiO_2-S-Pd_{SA} (Figures S5 and S6, respectively).

X-ray absorption spectroscopy (XAS) was employed to investigate Pd's coordination environment in SiO_2-NH_2/Pd_{SA} and SiO_2-S-Pd_{SA} (Figure 1E, F). Figure 1E presents Pd K-edge X-ray absorption near-edge structure (XANES) spectra of SiO_2-NH_2/Pd_{SA} and SiO_2-S-Pd_{SA}. Accordingly, the absorption edge position in the spectrum for both SiO_2-S-Pd_{SA} and SiO_2-NH_2/Pd_{SA} sits between Pd foil and PdO (as references), suggesting that Pd species in both samples were to some extent oxidized, though cannot be claimed entirely.[22] The EXAFS analysis for both SiO_2-NH_2/Pd_{SA} and SiO_2-S-Pd_{SA} exhibits a single peak around $r = \sim 2$ Å (without phase shift correction), which is different from the case of Pd foil and PdO crystal, indicating a lack of long-range periodicity and therefore, demonstrating Pd species are separately coordinated to the N and S, respectively.

Curve-fitting analyses of the EXAFS results are also summarized in Table S3. The analysis revealed that SiO_2-NH_2/Pd_{SA} contains a Pd–N contribution, with a bond length of 2.06 Å and a coordination number (CN) of 4.0. In contrast, SiO_2-S-Pd_{SA} contains a Pd–S contribution, with a slightly longer bond length of 2.30 Å and a similar CN of 4.3. These results suggest that Pd species in both samples are highly dispersed and coordinated by the grafted ligands.

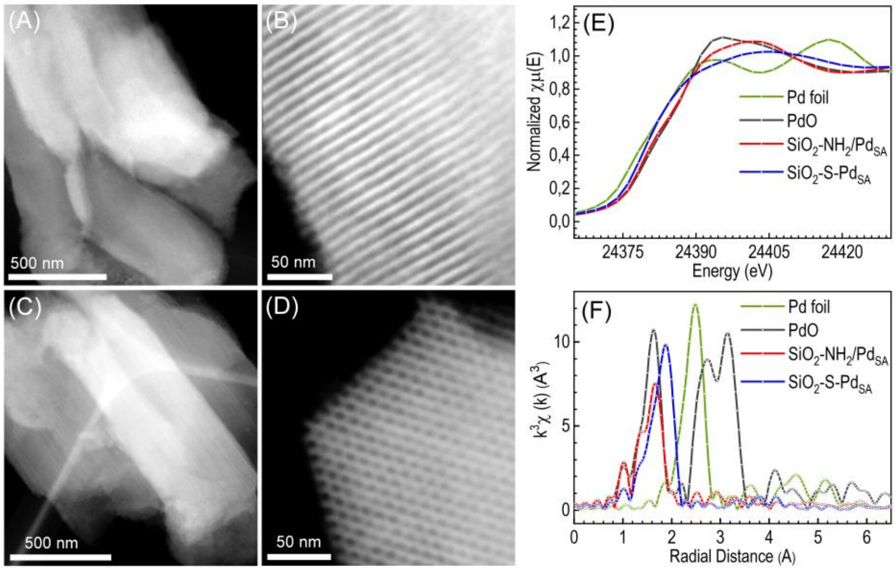

Figure 1. Low-magnified and high-magnified HAADF-STEM images of (A, B) SiO_2-NH_2/Pd_{SA}, (C, D) SiO_2-S-Pd_{SA}. Pd K-edge (E) XANES and (F) FT-EXAFS of SiO_2-S-Pd_{SA}, SiO_2-NH_2/Pd_{SA}, and reference materials (PdO and Pd foil).

UV-vis reflectance spectra (Figure S7) also show that there is a chemical bonding between Pd and S/N, in which the Pd-S bonding has caused a significant enhancement in light absorption. Two characteristic peaks at 260 nm in SiO_2-S-Pd_{SA} and 272 nm in SiO_2-NH_2/Pd_{SA}, are assignable to the ligand-centered transitions.[31] A peak in SiO_2 (205 nm), SiO_2-NH_2/Pd (209 nm), and SiO_2-S-Pd_{SA} (213 nm) is also observed with a slight shift but an identical nature as characteristic of the SiO_2 substrate structure.[9,32] SiO_2-S-Pd_{SA} indicates one extra and intense broadband at $\lambda_{max} = 387$ nm, hinting at the strong coordination of -SH groups to Pd through d-d transition and ligand-to-metal-charge-transition (LMCT),[33,34] further demonstrating that in SiO_2-S-Pd_{SA}, Pd species experience a fundamentally different coordination and bonding environment. The presence of LMCT-relevant peaks in thiol-to-Pd coordinated materials also shows that the Pd species in these materials are either in the form of clusters or single atoms since nanoparticles usually show weak-to-no peaks related to the LMCT.[9,35]

We also synthesized Pd_{SA} loaded on dithiocarbamate-functionalized SiO_2 (SiO_2-$NHCS_2H$-Pd_{SA},) *via* the treatment of the -NH_2 functional groups of SiO_2-NH_2 with CS_2 to convert NH_2 into -$NHCS_2H$ groups and the subsequent Pd deposition. Likewise, ^{29}Si MAS NMR and HAADF-STEM revealed the grafting of the $NHCS_2H$ functional group on SBA-15 and subsequent Pd_{SA} loading (Figure S8A, B). The XAS results of SiO_2-$NHSC_2$-Pd are in Figure S9. Accordingly, the absorption edge position of Pd in SiO_2-$NHSC_2$-Pd_{SA} is similar to that of the Pd species in SiO_2-S-Pd, where the calculated bond length from EXAFS results is found to be 2.33 Å (Table S3). All the results described above indicate the successful loading of single-atom Pd on a mesoporous silica with only difference in organic functional groups (linkers) between the Pd and the silica surface in SiO_2-NH_2/Pd_{SA}, SiO_2-S-Pd_{SA}, and SiO_2-$NHCS_2H$-Pd_{SA}, which must be helpful to investigate how the supporting environments of single-atom Pd affect its catalytic performance and stability.

Catalytic activity study

Here, we selected formic acid (FA) dehydrogenation as a case catalytic reaction since FA is a facile H_2 storing agent that can form by reacting H_2 with CO_2 and catalytically regenerating H_2 with a metal-based catalyst such as Ir, Ru, Pd.[12,36–38] We compared the catalytic activities of SiO_2-NH_2/Pd_{SA} and SiO_2-S-Pd_{SA} in the catalytic dehydrogenation of FA under identical reaction conditions. Accordingly, SiO_2-S-Pd_{SA} exhibited a lower H_2 production yield during the monitored reaction time (90 min) than the SiO_2-NH_2/Pd_{SA} (Figure 2A). Furthermore, the turnover frequency (TOF, h^{-1}) of SiO_2-NH_2/Pd_{SA} was obtained at 104.8 h^{-1}, which is 7.6 folds higher than that of SiO_2-S-Pd_{SA} (13.8 h^{-1}) (Figure 2B) at 70 ^{o}C. As the reaction temperature downs to room temperature (22 ^{o}C), the catalytic activity gap between SiO_2-NH_2/Pd_{SA} (47.14 h^{-1}) and SiO_2-S-Pd_{SA} (1.6 h^{-1}) increased to 29.5 folds higher catalytic activity (Figure S10). Further, the Pd wt% on SiO_2-NH_2 was also optimized by testing several loading amounts and different catalyst quantities in the reaction. As shown in Figure S11, the optimal Pd wt% was 1.8 wt%, and the optimal amount of 1.8 wt% SiO_2-NH_2/Pd_{SA} was 10 mg to 5 mL FA (5 V/V%).

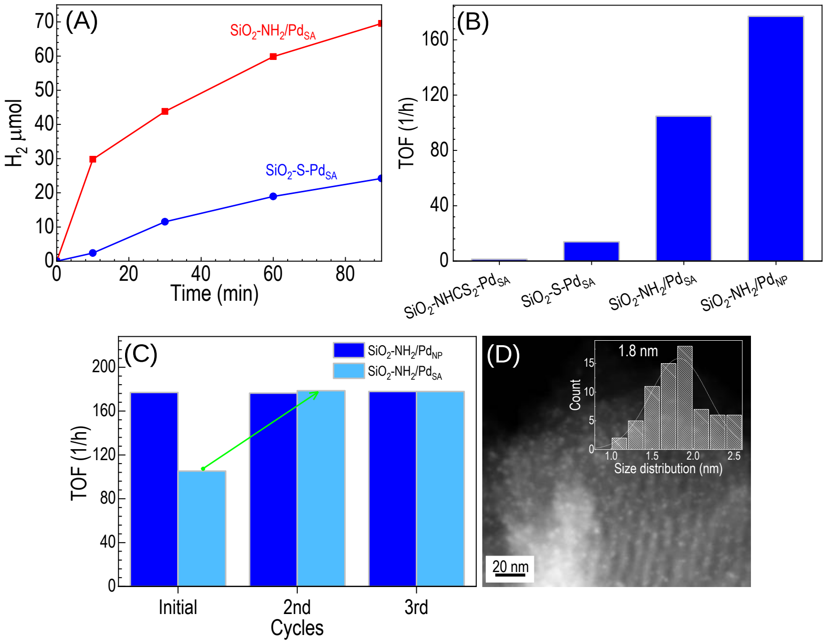

Figure 2. (A) Comparing the catalytic dehydrogenation activity of the SiO_2-S-Pd_{SA} and SiO_2-NH_2/Pd_{SA} at 70 °C through FA (5 V/V%). (B) Comparing the TOF values of different single-atom Pd catalysts with SiO_2-NH_2/Pd_{NP} in FA dehydrogenation at 70 °C. (C) Recyclability study of SiO_2-NH_2/Pd_{SA} and SiO_2-NH_2/Pd_{NP} in FA acid dehydrogenation at 70 °C. HAADF-STEM image of the recovered SiO_2-NH_2/Pd_{SA} after FA dehydrogenation reaction. The inset shows the particle size distribution of the Pd nanoparticles.

We hypothesize that this difference in the catalytic activity is because of the interplay between Pd and functional groups. To probe the suppressive role of thiol, we examined the catalytic activity of SiO_2-$NHCS_2$-Pd_{SA} under identical conditions to that of SiO_2-S-Pd_{SA}. The -$NHCS_2H$ group is similar to -SH, being terminated with functional sulfur, and is expected to react with Pd like the thiol group. The observed catalytic activity (TOF = 1.7 h^{-1}) for SiO_2-$NHCS_2$-Pd_{SA} was even lower than SiO_2-S-Pd_{SA} (Figure 2B). This lower catalytic activity might be because the dithiocarbamate ligand in SiO_2-$NHCS_2$-Pd has two sulfur atoms in resonance with each other and the amine, making Pd-S bonds more covalent type and less active in the catalysis.[39,40]

To demonstrate if the observed superior catalytic activity in SiO_2-NH_2/Pd_{SA} can be correlated with the anime group's basicity, regardless of what has been coordinated to Pd species, during the catalysis by SiO_2-S-Pd_{SA}, we added propylamine compound, which corresponds to that of the functionalized propylamine in SiO_2-NH_2/Pd_{SA}. As shown in Figure S12, the added amine groups had a minor effect on the catalytic activity (from 13.8 h^{-1} to 18.5 h^{-1}), indicating that amine basicity is not a critical factor in determining the Pd species' catalytic activity.

Structural transformations and stability of Pd_{SA} on functionalized silica

To investigate the stability of atomically dispersed Pd within the silica matrices, we post-treated each of the SiO_2-S-Pd_{SA} and SiO_2-NH_2/Pd_{SA} samples with different methods, trying to understand the stability of Pd_{SA} in exposure to different reactive compounds. In SiO_2-NH_2/Pd_{SA}, after treating with concentrated $NaBH_4$, Pd_{SA} converted into Pd_{NP}, observable under the STEM (Figure S13). Accordingly, the TOF of SiO_2-NH_2/Pd_{NP} was found to be 177.0 h^{-1}, which is even higher than that of SiO_2-NH_2/Pd_{SA} (Figures 2B and S14) and is close to that of the recovered SiO_2-NH_2/Pd_{SA} (TOF = 178.5 h^{-1}, Figure 2C).

In SiO_2-S-Pd_{SA}, the sample was first treated with a relatively harsh oxidating agent (i.e., H_2O_2), which detached the coordinated Pd_{SA} from thiol groups through oxidating -SH to -SO_3H groups (Figure S15). HAADF-STEM observation and low-angle XRD results after H_2O_2 treatment showed the aggregation of Pd species and considerable destruction of the mesoscopic structures. Despite the destruction and accumulation, the H_2O_2-caused S-Pd bond breaking led to a better activity than the pristine sample (SiO_2-S-Pd_{SA}) in catalytic formic acid dehydrogenation (Figure S16). This investigation also shows that the Pd-S coordination is detrimental to the catalytic efficiency of Pd. Unlike SiO_2-NH_2/Pd_{SA}, when SiO_2-S-Pd_{SA} was treated with $NaBH_4$ under identical conditions, no Pd aggregation was found under HAADF-STEM observation, showing that the Pd-S is more resistant to reducing agent than the Pd-N bond.

We now consider the positive role of amine functionality in Pd catalysis. The TEM image of the recovered SiO_2-NH_2/Pd_{SA} from the first run (Figure 2D) shows that Pd species in the recovered SiO_2-NH_2/Pd_{SA} have aggregated into nanoparticles, averaging in size ~1.8 nm (inset of Figure 2D) during the FA dehydrogenation reaction at 70 °C. The extent of such aggregation depends on the type of functional group coordinating with Pd and the reaction conditions (e.g., temperature). Our previous studies about Pd thickness optimization on silicate sheets show that such a particle size can exhibit excellent metallicity and catalytic activity.[10] The recovered SiO_2-NH_2/Pd_{SA} from the first run, in which the Pd_{SA} is converted into nanoparticles, exhibits a higher activity than the initial sample. Eventually, the catalytic activity stabilizes in the further runs under identical reaction conditions. The *in situ*-generated Pd_{NP} (TOF = 178.5 h^{-1}) reveals better catalytic behavior than the SiO_2-NH_2/Pd_{SA} (104.8 h^{-1}). The low catalytic activity of single atom Pd species appears in the early minutes of the catalysis of SiO_2-NH_2/Pd_{SA}—the interval that Pd_{SA} converts into Pd_{NP} to start the catalytic reaction.

Again, unlike the recovered SiO_2-NH_2/Pd_{SA}, the recovered SiO_2-S-Pd_{SA} showed no Pd aggregation during the formic acid dehydrogenation, judging from TEM observation (Figure S17) and wide angle XRD pattern (Figure S18). XPS further confirmed the high Pd_{SA} stability on the thiol functional group for the overall structure, where the Pd's 3*d* peak positions have slightly changed compared to the pristine ones (discussed later in Figure 3). It can be inferred that when the Pd_{SA} is coordinated with the thiol, the Pd-S ligand bond is more stable than the Pd-N bond, so the Pd species is more inert toward FA. In conclusion, Pd_{SA}'s instability or mobility on a functionalized surface can be crucial in determining its catalytic activity. In conclusion, the recovered SiO_2-NH_2/Pd_{SA}—as Pd *in situ*-generated nanoparticles' representative—reveal a superior activity than SiO_2-S-Pd_{SA}—assumed as the Pd single atoms' representative.

The investigated wide-angle XRD patterns of Pd_{SA}-based catalysts (before and after FA dehydrogenation reaction recovery from the reactions indicated no relevant Pd diffraction pattern peak, although the recovered SiO_2-NH_2/Pd is composed of nanoparticles/clusters (Figure S18). This result shows that the Pd nanoparticles, during formic acid dehydrogenation, do not reach a particle size or crystal structure that could generate a diffraction pattern. Furthermore, in the long-term exposure of the catalyst in the reaction, the catalyst surface may deal with some surface deactivation that can be readily reactivated by heat treating at 80–90 °C for 20 min (experimental section). This reactivation method shows that the surface of Pd species is probably hindered by (side) product molecules that suppress the catalytic activity by surface blockade. Therefore, the catalytic activity can be reverted to the initial state by heating the sample and desorbing the compounds attached to the surface.

Ex-situ catalytic mechanism investigation with XPS

We further studied the catalytic mechanisms of SiO_2-NH_2/Pd_{SA} and SiO_2-S-Pd_{SA} with X-ray photoelectron spectroscopy (XPS) measurement of Pd 3*d*. Since Pd(0) binding energy (BE) does not fairly shift in different media,[41] while ionic Pd's BE significantly shifts depending on the ligand type, we assigned a constant value to Pd(0) in the Pd_{SA}-loaded samples, while the ionic Pd species were assigned to variable BEs. In the case of SiO_2-NH_2/Pd_{SA} and SiO_2-NH_2/Pd_{NP}, the BE of 334.1 eV was assigned to Pd(0), and all the spectra were fitted accordingly. In the case of SH-contained samples, the Pd(0) BE was also assigned to a constant value, and all peaks were fitted accordingly.

According to the fitted results from SiO_2-NH_2/Pd_{SA}, a maximum of ~7% of Pd species can be attributed to the Pd(0) species. However, after reducing with $NaBH_4$ (SiO_2-NH_2/Pd_{NP}), the Pd(0) fraction increases up to 31%. Moreover, the abundance of the assigned peak of Pd(0) in the recovered SiO_2-NH_2/$Pd_{SA,}$ after the formic acid dehydrogenation reaction, reaches up to 75%. The reduction of ionic Pd during the reaction shows that Pd single atoms on amine functional groups are mobile enough to migrate and aggregate into nanoparticles (Figure 3). A slight shift in ionic Pd peaks for SiO_2-NH_2/Pd samples is because ionic Pd's coordination with the -NH_2 functional group is looser and, besides, can bond with the other species such as surface silanols or other guest molecules (*e.g.*, formate after from the solution). In contrast, SiO_2-S-Pd_{SA} shows a stronger BE than SiO_2-NH_2/Pd_{SA}, and the peak positions of ionic Pd do not shift remarkably after the catalytic process (Figure 3).

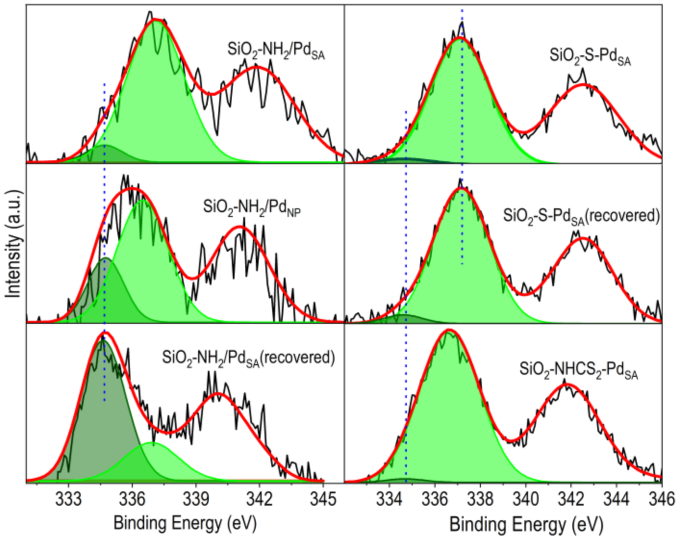

Figure 3. Pd 3*d* XPS spectra of SiO_2-NH_2/Pd_{SA}, SiO_2-NH_2/Pd_{NP}, recovered SiO_2-NH_2/Pd_{SA}, SiO_2-S-Pd_{SA}, Recovered SiO_2-S-Pd_{SA}, and SiO_2-$NHCS_2$-Pd_{SA}. Forest green is representative of Pd(0) and lawn green shows ionic Pd.

The XPS spectrum of SiO_2-S-Pd_{SA} after the recovery from the reaction mixture still shows the ionic Pd as majorly retained (>~98%), compared to the pristine SiO_2-S-Pd_{SA}. This resistivity in reducing ionic Pd during the reaction on the SH-type functional group shows that the Pd species are strongly bonded with the SH species and are not mobile-like -NH_2 functional group. Therefore, by looking at the catalytic activity (Figure 2A) and the transformability of ionic Pd to Pd(0) in SiO_2-NH_2/Pd_{SA} and SiO_2-S-Pd_{SA} through XPS (Figure 3) and TEM results (Figure 2D and Figure S13), it can be concluded that the more bond strength between Pd and the functional group is, the less catalytic activity would be obtained in the FA dehydrogenation reaction.

It is also noteworthy that when the Pd is bonded to the dithiocarbamate, the BE of ionic Pd slightly shifts to lower BE, compared to the -SH functional group, which is due to the resonance between thiocarbonyl, -SH groups, and the amine (Figure 3).[40] However, both thiol-based functional groups show a minor amount of Pd(0) in the structure, while the amino-based structure shows a higher fraction of Pd(0) in the pristine form.

Density Functional Investigations

Our TEM and XAS results indicate that, at least for the first catalytic cycle, most Pd ions on both SiO_2-NH_2/Pd_{SA} and SiO_2-S-Pd_{SA} samples would likely be deposited as single atoms instead of agglomerating to form Pd nanoparticles. Considering that Pd ions on SiO_2-NH_2 and SiO_2-SH behave radically differently, we infer that the interplay between Pd ions and the functional groups is critical to the catalytic performance. Here, we resort to density functional calculations to elucidate this interplay at the atomic level.

Figure 4A and Figure 4B show the optimized structures of a single Pd ion bonded to C_3H_6-NH_2 and C_3H_6-S- groups when attached to a silica substrate. In the SiO_2-NH_2/Pd_{SA} system, the Pd ion forms a bond with the N ion and relaxes to a position relatively far from the surface, taking a distance of 3.929 Å. Here, the Pd-N bond length is 2.079 Å, where there is a good agreement with the obtained bond length value from Pd K-edge XAS (2.06 Å, Table S3). Pd ion in the SiO_2-S-Pd_{SA} system, however, relaxes to a different geometry. In this case, although the C_3H_6-S-Pd group is stretched up to 3.353 Å away from the silica surface, the Pd ion falls closer to the silica surface, eventually~~,~~ forming a 2.256 Å bond with S. The calculated Pd-S bond length here is also well-matching the obtained value from Pd K-edge XAS (2.30 Å). Pd's interaction with the silica surface in the SiO_2-S-Pd_{SA} was not readily apparent at the start of our investigations. Before simulating the configuration in Figure 4B, we investigated a structure where all three outmost O on the silica surface were capped with H. However, after we realized Pd's tendency to relax toward the silica surface, we removed the capping H atom from the O towards which Pd relaxes, as oxygen is commonly coordinated by two cations. In this instance, those would be one Pd and one Si. The initial functional group configurations, without Pd loading, are shown in Figure S19, sharing many geometrical features with the one presented here, except that one of its surface oxygens is over-coordinated.

The stability of Pd's attachment to a functional group can be assessed by its formation energy (E^f), which is calculated by subtracting the total energy of a product from the total energies of its constituents. Using density functional energies instead to calculate the formation energies would be a viable approximation if the vibrational energies can be negligible. Accordingly, we calculated Pd's formation energy in SiO_2-NH_2/Pd_{SA} and SiO_2-S-Pd_{SA}, which indicates the Pd bond strength with the functional group, as:

$E^f(\mathrm{SiO_2\text{-}NH_2/Pd_{SA}}) = E_{\mathrm{DFT}}(\mathrm{SiO_2\text{-}NH_2/Pd_{SA}}) - E_{\mathrm{DFT}}(\mathrm{SiO_2\text{-}NH_2}) - \mu_{\mathrm{Pd}}$, Equation 1

$E^f(\mathrm{SiO_2\text{-}S\text{-}Pd_{SA}}) = E_{\mathrm{DFT}}(\mathrm{SiO_2\text{-}S\text{-}Pd_{SA}}) - E_{\mathrm{DFT}}(\mathrm{SiO_2\text{-}SH}) - \mu_{\mathrm{Pd}} + \mu_{\mathrm{H}}$. Equation 2

Here, E_{DFT} denotes the density functional energy for the system with and without Pd ions. The systems without Pd, *i.e.*, SiO_2-NH_2 and SiO_2-SH, are shown in Figure S19. μ_{Pd} and μ_{H} are palladium's and hydrogen's chemical potential, indicating the availability of these chemicals during the synthesis process. For instance, μ_{Pd} can take values between $E_{\mathrm{DFT}}(\mathrm{Pd}_{metallic}) < \mu_{\mathrm{Pd}} < 0$, where $E_{\mathrm{DFT}}(\mathrm{Pd}_{metallic})$ is the DFT energy of bulk metallic palladium per atom. Here, $\mu_{\mathrm{Pd}} = 0$ is the limit where no Pd is available, while $\mu_{\mathrm{Pd}} = E_{\mathrm{DFT}}(\mathrm{Pd}_{metallic})$ signifies the abundance of Pd, so any lower μ_{Pd} would make metallic Pd more stable than chelated Pd. Since the synthesis conditions for both single-atom bearing samples in our experiment were identical, the chemical potentials were taken to be the same in both equations. Moreover, since we are more interested in comparing the relative stability of Pd in these two configurations, the exact μ_{Pd} and μ_{H} were less critical to our goal. So, we set μ_{Pd} to be equal to metallic Pd's DFT energy and μ_{H} to be equal to half of the DFT energy of H_2 gas.

We obtained $E^f(\mathrm{SiO_2\text{-}NH_2/Pd_{SA}}) = -0.189$ eV, and $E^f(\mathrm{SiO_2\text{-}S\text{-}Pd_{SA}}) = -2.475$ eV. The relatively high E^f value for $\mathrm{SiO_2\text{-}NH_2/Pd_{SA}}$, which is equivalent to −18.268 KJ/mol, demonstrates that Pd is attached through weak physical adsorption (physisorption) to the amino-functionalized surface than that of the thiol-functionalized surface. In contrast, the lower E^f for $\mathrm{SiO_2\text{-}S\text{-}Pd_{SA}}$, which is equivalent to −238.806 KJ/mol, is at the stronger bound of chemical adsorption. Consequently, the Pd bond within the $\mathrm{SiO_2\text{-}S\text{-}Pd_{SA}}$ is substantially stronger, therefore, remains less disturbed by subsequent chemical reactions during catalysis.

The nature of Pd's bonding to functional groups can be further elucidated by analyzing the electronic localization function η.[42] η is the probability of finding more than one spin-like electron at a point. In essence, η measures the degree of electron localization and provides a way to visualize the distribution of electrons.[43] η values closer to zero indicate regions of low electron delocalization, and values closer to one indicate areas of high electron localization. As in Figure 4C and Figure 4E, η takes a global maximum near the anion and a global minimum at the bond center in Pd-N, Pd-S. This η profile indicates ionic bonding,[44] whose strength depends on the transferred charge. Bader charge analysis shows that Pd has 15.92 valance electrons in SiO_2-NH_2/Pd and 15.48 *e* in SiO_2-S-Pd. Note that the Pd pseudopotential contained 16 electrons,

$4p^6 4d^{10} 5s^0$. Lower Pd charge in SiO_2-S-Pd demonstrates a more significant charge transfer to S and O, resulting in stronger ionic bonding and higher chemical stability.

According to the Sabatier principle, a good catalyst must be able to bond to the adsorbate, formic acid in our case, and be able to release the catalytic products relatively easily. The first half of the Sabatier principle is directly related to the transition metal's ability to fill the adsorbate's antibonding orbitals, shown in Figure 4G.[45] To achieve this, a transition metal must have labile electrons in narrow *d* bands, not too far from the Fermi level.[20] To assess the electronic lability of Pd in SiO_2-NH_2/Pd_{SA} and SiO_2-S-Pd_{SA}, we integrated the Pd 4*d* states, shown in Figure 4D and Figure 4F, within the highlighted 3 eV window below the Fermi level. Electrons in this energy window are more likely to participate in electronic hybridization during the catalytic reactions.[10,20,46–48]

The SiO_2-NH_2/Pd_{SA} system had a total of 5.624 *e* labile electrons, while the SiO_2-S-Pd_{SA} system had 2.335 *e*, less than half of SiO_2-NH_2/Pd_{SA}, explaining the better catalytic performance observed. The larger labile electronic population in SiO_2/NH_2/Pd_{SA} can be explained by the lack of hybridization with N 2*s* and 2*p* states, as filled N 2*s* and 2*p* states are concentrated at energies lower than −4 eV and empty N 2*p* states are far above the Fermi level at ~2 eV. This lack of hybridization leaves the Pd 4*d* states metallic-like, gravitating to the vicinity of the Fermi level.[49] In SiO_2-S-Pd_{SA}, Pd 4d states hybridize strongly with filled *s* and *p* states from both O and S in the region -7 eV $< E < -3$ eV, evidenced by many overlapping peaks. Consequently, the 4*d* states distribution over the energy range becomes more like a chalcogenide compound where a great deal of 4*d* states is pulled to lower energies.[50]

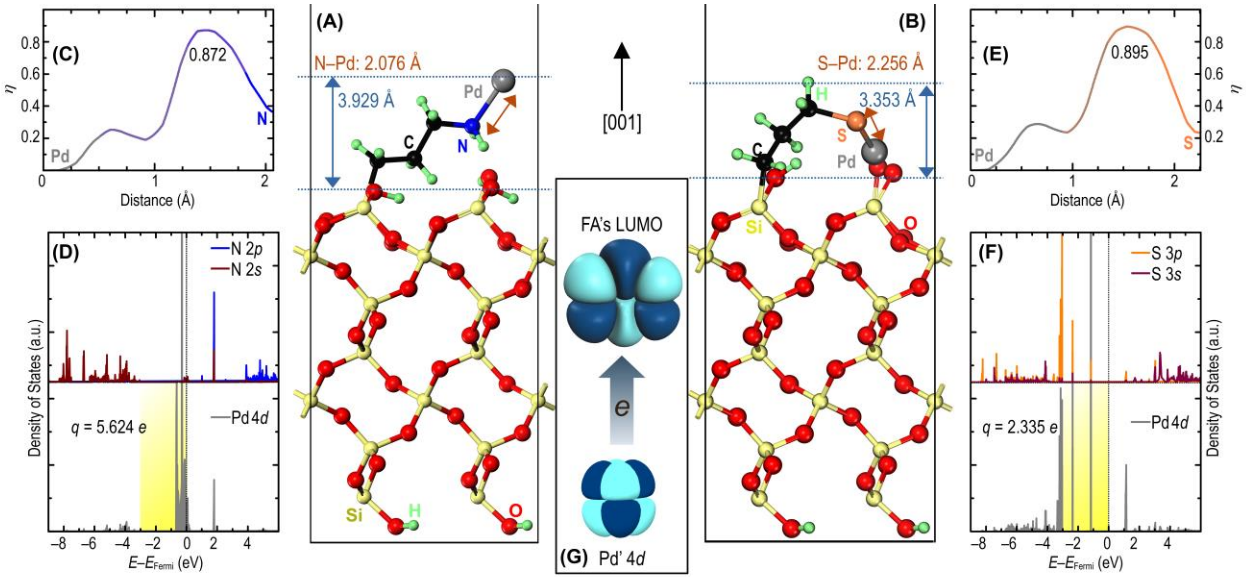

Figure 4. (A) and (B) The optimized structure of the SiO_2-NH_2/Pd_{SA} and SiO_2-S-Pd_{SA}. (C) The electronic localization function (η) along the Pd-N bond in SiO_2-NH_2/Pd_{SA}. (D) The partial density of states of Pd 4*d* and its coordinating N 2*s* and 2*p* in SiO_2-NH_2/Pd_{SA}. (E) The electronic localization function (η) along the Pd-S bond in SiO_2-SPd_{SA}. (F) The partial density of states of Pd 4*d* and coordinating S 3*s* and 3*p* along with 2*p* in SiO_2-S-Pd_{SA}. (G) Charge transfer mechanism from Pd catalyst to formic acid's lowest unoccupied orbital facilitating the catalytic reaction.

Conclusion

The electronic interaction between single atom Pd (Pd_{SA}) and different functional groups on mesoporous silica was investigated to determine the effect of a functional group on the catalytic activity of Pd_{SA} in formic acid dehydrogenation reaction. Comprehensive spectral analyses (synchrotron XAS and XPS) and TEM observations showed that the oxidation state of Pd_{SA} loaded on the amine functional group can readily change from ionic to Pd(0), while in the case of thiol-based functional groups, the oxidation state of Pd barely changes. Additionally, we observed an inverse relationship between Pd_{SA}'s catalytic activity and the stability of its oxidation state caused by the aggregation into nanoparticles during the reaction. The position of Pd's 4*d* states with respect to the Fermi level can explain the catalytic behavior. When Pd's 4*d* states concentrate closer to the Fermi level, they become more labile for catalytic activity. This occurs when the Pd bond with the functional group involves little to no charge transfer or when

Pd ions aggregate to form metallic nanoparticles. Both these scenarios manifest in the case of Pd atoms loaded on amine functional groups. In contrast, when the bond between Pd and the functional group is more ionic, more of Pd's 4*d* states are pulled to deeper energy levels away from the Fermi level. In such a case, the deeper 4*d* states do not participate in catalysis. Stronger Pd-ligand bonding also prevents Pd aggregation into metallic nanoparticles. The latter case describes the behavior of Pd_{SA} loaded in thiol groups.

Associated content

The Supporting Information is available free of charge at https://pubs.acs.org/doi/10.1021/acsami.XXX.
Further details about the experimental section, including chemical and apparatus, XPS measurement, EXAFS/XANES measurements, synthesis of thiofunctionalized SiO_2 (SiO_2-SH), synthesis of aminofunctionalized SiO_2 (SiO_2-NH_2), Synthesis of single atom Pd_{SA}, synthesis of dithiocarbamate-functionalized SiO_2 (SiO_2-$NHCS_2H$), post-modification SiO_2-NH_2/Pd_{SA} and SiO_2-S-Pd_{SA}, catalytic tests, and computational methods; and further information about ^{29}Si MAS NMR and ^{13}C CP MAS NMR spectra, TG-DTA curves, low-angle XRD patterns, N_2 adsorption-desorption isotherms, HAADF-STEM images (including TEM-based elemental mappings) and UV-Vis spectra of SiO_2-S-Pd_{SA} and SiO_2-NH_2/Pd_{SA}, characterizations of post-treated SiO_2-NH_2/Pd_{SA} and SiO_2-S-Pd_{SA}, further catalytic dehydrogenation of FA under different conditions, characterizations of recovered samples, and the optimized model structures without Pd are available in the Supporting Information.

Acknowledgments

This work was supported by JSPS KAKENHI (Grant Numbers 21H02034). This work was also supported by the Joint Usage/Research Center for Catalysis. The XAS measurements were performed at BL14B2 of SPring-8 (proposal No. 2022A1827). E. D. acknowledges the TÜBİTAK and Horizon-2020 Marie Skłodowska Curie for providing financial support in Co-Funded Brain Circulation Program (Project No. 120C057) framework.

Reference

(1) Koga, Y.; Kaneda, T.; Saito, Y.; Murakami, K.; Itami, K. Synthesis of Partially and Fully Fused Polyaromatics by Annulative Chlorophenylene Dimerization. *Science* **2018**, *359* (6374), 435–439. https://doi.org/10.1126/science.aap9801.

(2) Trost, B. M.; Huang, Z.; Murhade, G. M. Catalytic Palladium-Oxyallyl Cycloaddition. *Science* **2018**, *362* (6414), 564–568. https://doi.org/10.1126/science.aau4821.

(3) Kiss, G. Palladium-Catalyzed Reppe Carbonylation. *Chem. Rev.* **2001**, *101* (11), 3435–3456.

(4) Motokura, K.; Ding, S.; Usui, K.; Kong, Y. Enhanced Catalysis Based on the Surface Environment of the Silica-Supported Metal Complex. *ACS Catal.* **2021**, *11* (19), 11985–12018. https://doi.org/10.1021/acscatal.1c03426.

(5) Martis, M.; Mori, K.; Fujiwara, K.; Ahn, W.-S.; Yamashita, H. Amine-Functionalized MIL-125 with Imbedded Palladium Nanoparticles as an Efficient Catalyst for Dehydrogenation of Formic Acid at Ambient Temperature. *J. Phys. Chem. C* **2013**, *117* (44), 22805–22810. https://doi.org/10.1021/jp4069027.

(6) Zhang, J.; Liao, W.; Zheng, H.; Zhang, Y.; Xia, L.; Teng, B.-T.; Lu, J.-Q.; Huang, W.; Zhang, Z. Morphology-Engineered Highly Active and Stable Pd/TiO2 Catalysts for CO2 Hydrogenation into Formate. *J. Catal.* **2022**, *405*, 152–163. https://doi.org/10.1016/j.jcat.2021.11.035.

(7) Wen, M.; Mori, K.; Kuwahara, Y.; Yamashita, H. Plasmonic Au@Pd Nanoparticles Supported on a Basic Metal–Organic Framework: Synergic Boosting of H2 Production from Formic Acid. *ACS Energy Lett.* **2017**, *2* (1), 1–7. https://doi.org/10.1021/acsenergylett.6b00558.

(8) Wang, Z.; Liang, S.; Meng, X.; Mao, S.; Lian, X.; Wang, Y. Ultrasmall PdAu Alloy Nanoparticles Anchored on Amine-Functionalized Hierarchically Porous Carbon as Additive-Free Catalysts for Highly Efficient Dehydrogenation of Formic Acid. *Appl. Catal., B* **2021**, *291*, 120140. https://doi.org/10.1016/j.apcatb.2021.120140.

(9) Wang, N.; Sun, Q.; Bai, R.; Li, X.; Guo, G.; Yu, J. In Situ Confinement of Ultrasmall Pd Clusters within Nanosized Silicalite-1 Zeolite for Highly Efficient Catalysis of Hydrogen Generation. *J. Am. Chem. Soc.* **2016**, *138* (24), 7484–7487. https://doi.org/10.1021/jacs.6b03518.

(10) Doustkhah, E.; Tsunoji, N.; Assadi, M. H. N.; Ide, Y. Pd Thickness Optimization on Silicate Sheets for Improving Catalytic Activity. *Adv. Mater. Interfaces* **2023**, *10* (4), 2202368. https://doi.org/10.1002/admi.202202368.

(11) Lim, B.; Xia, Y. Metal Nanocrystals with Highly Branched Morphologies. *Angew. Chem., Int. Ed.* **2011**, *50* (1), 76–85. https://doi.org/10.1002/anie.201002024.

(12) Doustkhah, E.; Hasani, M.; Ide, Y.; Assadi, M. H. N. Pd Nanoalloys for H2 Generation from Formic Acid. *ACS Appl. Nano Mater.* **2020**, *3* (1), 22–43. https://doi.org/10.1021/acsanm.9b02004.

(13) Gao, F.; Goodman, D. W. Pd–Au Bimetallic Catalysts: Understanding Alloy Effects from Planar Models and (Supported) Nanoparticles. *Chem. Soc. Rev.* **2012**, *41* (24), 8009–8020. https://doi.org/10.1039/C2CS35160A.

(14) Chen, P.; Khetan, A.; Yang, F.; Migunov, V.; Weide, P.; Stürmer, S. P.; Guo, P.; Kähler, K.; Xia, W.; Mayer, J.; Pitsch, H.; Simon, U.; Muhler, M. Experimental and Theoretical Understanding of Nitrogen-Doping-Induced Strong Metal–Support Interactions in Pd/TiO2 Catalysts for Nitrobenzene Hydrogenation. *ACS Catal.* **2017**, *7* (2), 1197–1206. https://doi.org/10.1021/acscatal.6b02963.

(15) Weerachawanasak, P.; Mekasuwandumrong, O.; Arai, M.; Fujita, S.-I.; Praserthdam, P.; Panpranot, J. Effect of Strong Metal–Support Interaction on the Catalytic Performance of Pd/TiO2 in the Liquid-Phase Semihydrogenation of Phenylacetylene. *J. Catal.* **2009**, *262* (2), 199–205. https://doi.org/10.1016/j.jcat.2008.12.011.

(16) Ament, K.; Köwitsch, N.; Hou, D.; Götsch, T.; Kröhnert, J.; Heard, C. J.; Trunschke, A.; Lunkenbein, T.; Armbrüster, M.; Breu, J. Nanoparticles Supported on Sub-Nanometer Oxide Films: Scaling Model Systems to Bulk Materials. *Angew. Chem., Int. Ed.* **2021**, *60* (11), 5890–5897. https://doi.org/10.1002/anie.202015138.

(17) Du, L.; Qian, K.; Zhu, X.; Yan, X.; Kobayashi, H.; Liu, Z.; Lou, Y.; Li, R. Interface Engineering of Palladium and Zinc Oxide Nanorods with Strong Metal–Support Interactions for Enhanced Hydrogen Production from Base-Free Formaldehyde Solution. *J. Mater. Chem. A* **2019**, *7* (15), 8855–8864. https://doi.org/10.1039/C8TA12019F.

(18) Saptal, V. B.; Ruta, V.; Bajada, M. A.; Vilé, G. Single-Atom Catalysis in Organic Synthesis. *Angewandte Chemie International Edition* **2023**, *62* (34), e202219306. https://doi.org/10.1002/anie.202219306.

(19) Xu, H.; Zhao, Y.; Wang, Q.; He, G.; Chen, H. Supports Promote Single-Atom Catalysts toward Advanced Electrocatalysis. *Coord. Chem. Rev.* **2022**, *451*, 214261. https://doi.org/10.1016/j.ccr.2021.214261.

(20) Greiner, M. T.; Jones, T. E.; Beeg, S.; Zwiener, L.; Scherzer, M.; Girgsdies, F.; Piccinin, S.; Armbrüster, M.; Knop-Gericke, A.; Schlögl, R. Free-Atom-like d States in Single-Atom Alloy Catalysts. *Nat. Chem.* **2018**, *10* (10), 1008–1015. https://doi.org/10.1038/s41557-018-0125-5.

(21) Shan, J.; Ye, C.; Jiang, Y.; Jaroniec, M.; Zheng, Y.; Qiao, S.-Z. Metal-Metal Interactions in Correlated Single-Atom Catalysts. *Sci. Adv.* **2022**, *8* (17), eabo0762. https://doi.org/10.1126/sciadv.abo0762.

(22) Finzel, J.; Sanroman Gutierrez, K. M.; Hoffman, A. S.; Resasco, J.; Christopher, P.; Bare, S. R. Limits of Detection for EXAFS Characterization of Heterogeneous Single-Atom Catalysts. *ACS Catal.* **2023**, 6462–6473. https://doi.org/10.1021/acscatal.3c01116.

(23) Li, R.; Wang, D. Understanding the Structure–Performance Relationship of Active Sites at Atomic Scale. *Nano Research* **2022**, *15* (8), 6888–6923. https://doi.org/10.1007/s12274-022-4371-x.

(24) Liu, J.; Zou, Y.; Cruz, D.; Savateev, A.; Antonietti, M.; Vilé, G. Ligand–Metal Charge Transfer Induced via Adjustment of Textural Properties Controls the Performance of Single-Atom Catalysts during Photocatalytic Degradation. *ACS Appl. Mater. Interfaces* **2021**, *13* (22), 25858–25867. https://doi.org/10.1021/acsami.1c02243.

(25) Gan, T.; Wang, D. Atomically Dispersed Materials: Ideal Catalysts in Atomic Era. *Nano Research* **2023**. https://doi.org/10.1007/s12274-023-5700-4.

(26) Bajada, M. A.; Di Liberto, G.; Tosoni, S.; Ruta, V.; Mino, L.; Allasia, N.; Sivo, A.; Pacchioni, G.; Vilé, G. Light-Driven C–O Coupling of Carboxylic Acids and Alkyl Halides over a Ni Single-Atom Catalyst. *Nature Synthesis* **2023**. https://doi.org/10.1038/s44160-023-00341-3.

(27) Zhang, Z.; Zhu, J.; Chen, S.; Sun, W.; Wang, D. Liquid Fluxional Ga Single Atom Catalysts for Efficient Electrochemical CO2 Reduction. *Angew. Chem., Int. Ed.* **2023**, *62* (3), e202215136. https://doi.org/10.1002/anie.202215136.

(28) Singh, B.; Sharma, V.; Gaikwad, R. P.; Fornasiero, P.; Zbořil, R.; Gawande, M. B. Single-Atom Catalysts: A Sustainable Pathway for the Advanced Catalytic Applications. *Small* **2021**, *17* (16), 2006473. https://doi.org/10.1002/smll.202006473.

(29) Vilé, G.; Albani, D.; Nachtegaal, M.; Chen, Z.; Dontsova, D.; Antonietti, M.; López, N.; Pérez-Ramírez, J. A Stable Single-Site Palladium Catalyst for Hydrogenations. *Angew. Chem., Int. Ed.* **2015**, *54* (38), 11265–11269. https://doi.org/10.1002/anie.201505073.

(30) Lettow, J. S.; Han, Y. J.; Schmidt-Winkel, P.; Yang, P.; Zhao, D.; Stucky, G. D.; Ying, J. Y. Hexagonal to Mesocellular Foam Phase Transition in Polymer-Templated Mesoporous Silicas. *Langmuir* **2000**, *16* (22), 8291–8295. https://doi.org/10.1021/la000660h.

(31) Xu, Y.; Claiden, P.; Zhu, Y.; Morita, H.; Hanagata, N. Effect of Amino Groups of Mesoporous Silica Nanoparticles on CpG Oligodexynucleotide Delivery. *Sci. Technol. Adv.* **2015**, *16* (4), 045006. https://doi.org/10.1088/1468-6996/16/4/045006.

(32) Jin, M.; Guo, Z.; Lv, Z. Immobilization of Tungsten Chelate Complexes on Functionalized Mesoporous Silica SBA-15 as Heterogeneous Catalysts for Oxidation of Cyclopentene. *J. Mater. Sci.* **2019**, *54* (9), 6853–6866. https://doi.org/10.1007/s10853-019-03361-7.

(33) Potter, M. E.; Le Brocq, J. J. M.; Oakley, A. E.; McShane, E. B.; Mhembere, P. M.; Carravetta, M.; Vandegehuchte, B. D.; Raja, R. Thiol Functionalised Supports for Controlled Metal Nanoparticle

Formation for Improved C–C Coupling. *Chem. Asian J.* **2021**, *16* (22), 3610–3614. https://doi.org/10.1002/asia.202100732.

(34) Yang, Z.; Smetana, A. B.; Sorensen, C. M.; Klabunde, K. J. Synthesis and Characterization of a New Tiara Pd(II) Thiolate Complex, [Pd(SC12H25)2]6, and Its Solution-Phase Thermolysis to Prepare Nearly Monodisperse Palladium Sulfide Nanoparticles. *Inorg. Chem.* **2007**, *46* (7), 2427–2431. https://doi.org/10.1021/ic061242o.

(35) Creighton, J. A.; Eadon, D. G. Ultraviolet–Visible Absorption Spectra of the Colloidal Metallic Elements. *J. Chem. Soc., Faraday Trans.* **1991**, *87* (24), 3881–3891. https://doi.org/10.1039/FT9918703881.

(36) Guan, C.; Zhang, D.-D.; Pan, Y.; Iguchi, M.; Ajitha, M. J.; Hu, J.; Li, H.; Yao, C.; Huang, M.-H.; Min, S.; Zheng, J.; Himeda, Y.; Kawanami, H.; Huang, K.-W. Dehydrogenation of Formic Acid Catalyzed by a Ruthenium Complex with an N,N′-Diimine Ligand. *Inorg. Chem.* **2017**, *56* (1), 438–445. https://doi.org/10.1021/acs.inorgchem.6b02334.

(37) Himeda, Y. Highly Efficient Hydrogen Evolution by Decomposition of Formic Acid Using an Iridium Catalyst with 4,4′-Dihydroxy-2,2′-Bipyridine. *Green Chem.* **2009**, *11* (12), 2018–2022. https://doi.org/10.1039/B914442K.

(38) Hull, J. F.; Himeda, Y.; Wang, W.-H.; Hashiguchi, B.; Periana, R.; Szalda, D. J.; Muckerman, J. T.; Fujita, E. Reversible Hydrogen Storage Using CO2 and a Proton-Switchable Iridium Catalyst in Aqueous Media under Mild Temperatures and Pressures. *Nat. Chem.* **2012**, *4* (5), 383–388. https://doi.org/10.1038/nchem.1295.

(39) von Wrochem, F.; Gao, D.; Scholz, F.; Nothofer, H.-G.; Nelles, G.; Wessels, J. M. Efficient Electronic Coupling and Improved Stability with Dithiocarbamate-Based Molecular Junctions. *Nat. Nanotech.* **2010**, *5* (8), 618–624. https://doi.org/10.1038/nnano.2010.119.

(40) Sauter, E.; Nascimbeni, G.; Trefz, D.; Ludwigs, S.; Zojer, E.; von Wrochem, F.; Zharnikov, M. A Dithiocarbamate Anchoring Group as a Flexible Platform for Interface Engineering. *Phys. Chem. Chem. Phys.* **2019**, *21* (40), 22511–22525. https://doi.org/10.1039/C9CP03306H.

(41) Moulder, J. F.; Stickle, W. F.; Sobol, P. E.; Bomben, K. D. *Handbook of X-Ray Photoelectron Spectroscopy; Perkin-Elmer Corporation: Eden Prairie, MN, 1992*; 1992.

(42) Becke, A. D.; Edgecombe, K. E. A Simple Measure of Electron Localization in Atomic and Molecular Systems. *J. Chem. Phys.* **1990**, *92* (9), 5397–5403. https://doi.org/10.1063/1.458517.

(43) Savin, A.; Nesper, R.; Wengert, S.; Fässler, T. F. ELF: The Electron Localization Function. *Angew. Chem., Int. Ed.* **1997**, *36* (17), 1808–1832. https://doi.org/10.1002/anie.199718081.

(44) Fuentealba, P.; Chamorro, E.; Santos, J. C. Chapter 5 Understanding and Using the Electron Localization Function. In *Theoretical and Computational Chemistry*; Toro-Labbé, A., Ed.; Elsevier, 2007; Vol. 19, pp 57–85. https://doi.org/10.1016/S1380-7323(07)80006-9.

(45) Nilsson, A.; Pettersson, L. G. M.; Hammer, B.; Bligaard, T.; Christensen, C. H.; Nørskov, J. K. The Electronic Structure Effect in Heterogeneous Catalysis. *Catal. Lett.* **2005**, *100* (3), 111–114. https://doi.org/10.1007/s10562-004-3434-9.

(46) Nørskov, J. K.; Abild-Pedersen, F.; Studt, F.; Bligaard, T. Density Functional Theory in Surface Chemistry and Catalysis. *Proc. Natl. Acad. Sci.* **2011**, *108* (3), 937–943. https://doi.org/10.1073/pnas.1006652108.

(47) Assadi, M. H. N.; Shigeta, Y. The Effect of Octahedral Distortions on the Electronic Properties and Magnetic Interactions in O3 NaTMO2 Compounds (TM = Ti–Ni & Zr–Pd). *RSC Adv.* **2018**, *8* (25), 13842–13849. https://doi.org/10.1039/C8RA00576A.

(48) Yeo, B. C.; Nam, H.; Nam, H.; Kim, M.-C.; Lee, H. W.; Kim, S.-C.; Won, S. O.; Kim, D.; Lee, K.-Y.; Lee, S. Y.; Han, S. S. High-Throughput Computational-Experimental Screening Protocol for the Discovery of Bimetallic Catalysts. *Npj Comput. Mater.* **2021**, *7* (1), 137. https://doi.org/10.1038/s41524-021-00605-6.

(49) Todorova, M.; Reuter, K.; Scheffler, M. Oxygen Overlayers on Pd(111) Studied by Density Functional Theory. *J. Phys. Chem. B* **2004**, *108* (38), 14477–14483. https://doi.org/10.1021/jp040088t.

(50) Blanco-Rey, M.; Jenkins, S. J. Methane Dissociation and Methyl Diffusion on PdO{100}. *J. Chem. Phys.* **2009**, *130* (1), 014705. https://doi.org/10.1063/1.3046683.

Graphical abstract: